An Analytical Study of Density Currents in Sheared, Stratified Fluids Including the Effects of Latent Heating

CHANGHAI LIU AND MITCHELL W. MONCRIEFF

National Center for Atmospheric Research, Boulder, Colorado*

(Manuscript received 18 September 1995, in final form 26 April 1996)

ABSTRACT

A nonlinear analytic model is used to study the bulk characteristics of energy conserving density currents in stratified and sheared environments. The idealized representation of latent heating in a stratified flow is a unique feature that interactively couples the dynamic and thermodynamic fields.

A stable stratification decreases the height of density currents but increases the corresponding propagation speed. In contrast, the density current is deeper and moves more slowly once latent heating is included. As for the effect of shear, the depth and the translation speed of density currents increase as the ambient shear varies from negative to positive (in the direction of propagation), with the exception of a strongly stable environment. A key addition to density current dynamics is the upper-level overturning circulation ahead of the system. This feature is very different from the blocked or choked upper-level structure found in the companion paper of Liu and Moncrieff. The distinction is attributed to the effect of different shear profiles on density current dynamics.

These analytic results quantifying the role of shear and latent heating in density-current-like phenomena in the atmosphere should now be evaluated against high-resolution numerical simulations and observations.

1. Introduction

Several atmospheric phenomena possess the morphological characteristics of the laboratory density current, such as thunderstorm outflows (e.g., Charba 1974; Goff 1976; Wakimoto 1982), sea and land breezes (e.g., Clarke 1961; Simpson 1969), certain cold fronts (e.g., Shapiro et al. 1985; Smith and Reeder 1988), and narrow rainbands (e.g., Carbone 1982; James and Browning 1979; Hobbs and Persson 1982). Some success has been reported in applying the density current theory and laboratory experiment results to these atmospheric processes—for example, their propagation speeds (e.g., Wakimoto 1982; Nicholls et al. 1988; Nielsen and Neilley 1990).

An obvious distinction between laboratory and atmospheric density currents regards stratification, although the unstratified approximation is acceptable in special circumstances. In previous theoretical studies (e.g., Benjamin 1968; Moncrieff and So 1989; Xu 1992; Xu and Moncrieff 1994) and laboratory experiments (e.g., Britter and Simpson 1978; Simpson and Britter 1979, 1980), the stratification influence is usually neglected. However, the absence of stratification in the dynamical formulation and experiment design is an issue in applying the results to atmospheric phenomena. Atmospheric density currents are further complicated by latent heat of condensation in convection initiated by dynamical forcing at the leading edge of the density current. This can locally modify the pressure field and thereby have a significant impact on the bulk properties of the density current.

This study is intended to investigate the effects of shear, base-state stratification, and latent heating. Section 2 describes the model of a steady density current; section 3 presents the features of density currents in a stratified but calm environment, especially the dynamical organization and propagation speed; in section 4 the analysis is extended to a sheared flow; section 5 is devoted to discussion; and finally, a summary and suggestions for future work are presented in section 6.

2. Steady model of a density current

The idealized steady-state density current model is schematically shown in Fig. 1, in which the flow is relative to a coordinate system moving at the travel speed of the density current. This model extends classic two-fluid density current theory by including stratification, shear, and latent heat of condensation. There is also a clear structural difference: the upward-displaced flow at the density current head flows rearward over the cold pool in the classic models such as Benjamin

* The National Center for Atmospheric Research is sponsored by the National Science Foundation.

Corresponding author address: Dr. Changhai Liu, Mesoscale and Microscale Meteorology Division, National Center for Atmospheric Research, P.O. Box 3000, Boulder, CO 80307-3000.
E-mail: chliu@ncar.ucar.edu

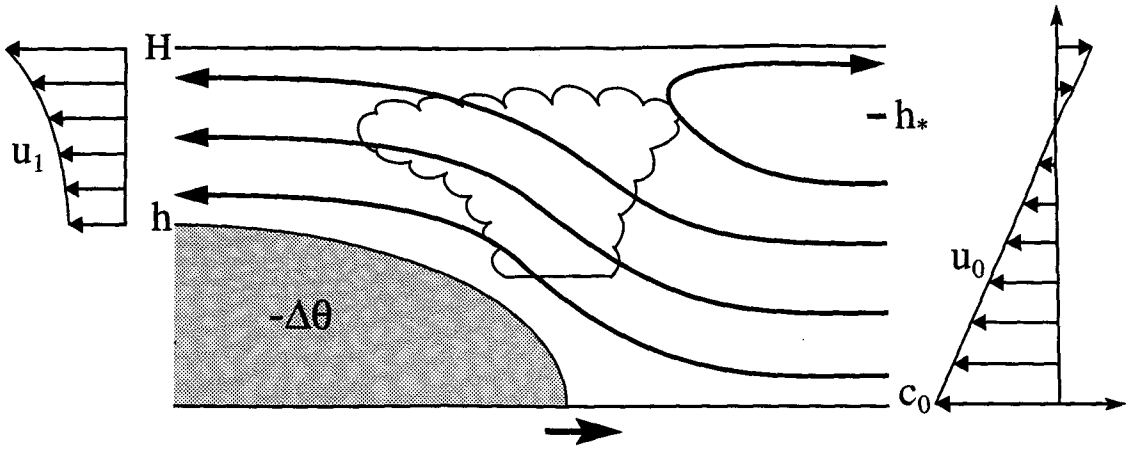

FIG. 1. Schematic of the relative flow in the steady analytic model. To the left and right of this diagram are plotted the asymptotic downstream and upstream wind fields, respectively. Here, $z = h_*$ is the steering level, which exists only if an overturning branch exists (i.e., in sufficiently strong ambient shear). The thick arrow denotes the direction of propagation of the system in ground-relative coordinates.

(1968), whereas in our models it contributes to an overturning current that flows *forward* at upper levels. This feature, shown in Fig. 1, occurs if the ambient shear is strong enough that the density current cannot travel faster than the flow at upper levels (i.e., it does not propagate). In this situation, the density current travels at the speed of the ambient flow at $z = h_*$, which is called a "steering level." The dynamic significance of this overturning branch in density currents was highlighted by Moncrieff and So (1989) and Liu and Moncrieff (1996).

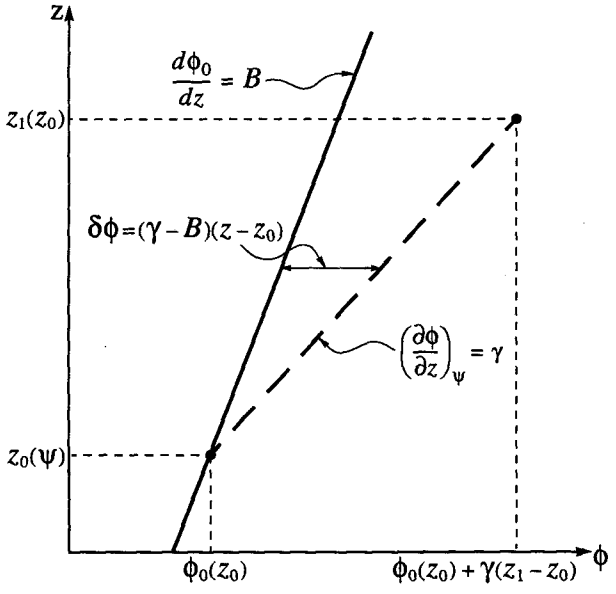

FIG. 2. Idealized parcel ascent. Rate of change of $\phi = \ln\theta$ along a parcel path is proportional to the vertical velocity. The ambient flow has a constant static stability B.

The density current is represented by a cold pool, of asymptotic height h, which has a potential temperature deficit, $-\Delta\theta(z)$, relative to a base state value $\theta_0(z)$. Furthermore, the cold air is motionless (in the relative frame of reference) so that the effect of cold pool dynamics is excluded. The remote inflow at z_0 is denoted by $u_0(z_0)$. The outflow shear is not equal to the inflow value because ascent in a stratified environment, and latent heating, causes tilting of the potential temperature surfaces, generating vorticity through the baroclinic effect. For simplicity, a constant value of $\Delta\theta(z)/\theta_0(z)$ is assumed. The height of the domain is H and the upper and lower boundaries are rigid, horizontal, and free-slip.

For analytical convenience, the following scaling is introduced to nondimensionalize the variables

$$\text{height} \quad H$$

$$\text{pressure} \quad \rho_0 g\left(\frac{\Delta\theta}{\theta_0}\right)H$$

$$\text{velocity} \quad \left[g\left(\frac{\Delta\theta}{\theta_0}\right)H\right]^{1/2}, \tag{1}$$

where ρ_0 is the reference air density and g the acceleration of gravity. The mathematical problem is made tractable by assuming steady, two-dimensional, incompressible, and inviscid flow and by neglecting the earth's rotation.

The static stability of the ambient flow is assumed to be a constant, $B = d\phi_0/dz$, where $\phi_0 = \ln\theta_0(z)$ is the log potential temperature of the base state. The approximation $D\phi/Dt \approx -LDq_s/c_pTDt$ follows from the second law of thermodynamics for moist convection, where $\phi = \ln\theta$ and other symbols have their traditional meaning. Since q_s is a function of temperature and

therefore mostly a function of height, it follows that $D\phi/Dt \approx -\Gamma w$ where $\Gamma = -L\partial q_s/c_pT\partial z$. Integration along trajectories gives $\phi(\psi, z) = \phi_0(z_0) - \int_{z_0}^{z} \Gamma dz$, where the integrand is evaluated along a trajectory (ψ), which is a streamline in steady flow. For simplicity we set $\Gamma = \gamma$ (a constant) although it is more accurately a function of (z, ψ).

It follows that, to a first approximation, the thermodynamic equation can be written as $D\phi/Dt = w\gamma$, which is a simple way to couple the thermodynamic and dynamic fields. Most important, the formulation allows the nonlinear thermodynamic equation to be integrated analytically in Lagrangian form along trajectories. This approach was used to study the dynamics of organized convection by Moncrieff and Green (1972), where further explanation can be found. Specifically, $\phi(\psi, z) = \phi_0(z_0) + \gamma(z - z_0)$, where $z_0(\psi)$ is the remote inflow height of the streamline (ψ) that can be related without further approximation to the outflow $z_1(z_0)$. Thus, the perturbation of the log potential temperature of an ascending air parcel from the base state value is $\delta\phi(\psi, z) = (\gamma - B)(z - z_0)$, at height z along a trajectory. The special case of $\gamma = 0$ represents adiabatic ascent in a dry stratified environment. The thermodynamics of the model is depicted in Fig. 2.

Another Lagrangian conservative quantity is the total energy $\frac{1}{2}v^2 + p/\rho_0 - \int \mathcal{B}dz = C(\psi)$, where $\mathcal{B} = g\,\delta\phi$ is the parcel buoyancy measured along particle paths and p is the perturbation of pressure from the base-state value. Note that $C(\psi)$ depends only on the streamfunction ψ, which, in the usual way, satisfies the conditions $u = \partial\psi/\partial z$ and $w = -\partial\psi/\partial x$. The equations for total energy, thermodynamic energy, and mass continuity (in the form $u_1 dz_1 = u_0 dz_0$, where u_1 is the remote outflow) can be combined into a "displacement equation" that functionally relates the inflow and outflow heights of streamlines. These arguments, together with additional conservative quantities that are not required here, are detailed in Moncrieff (1981).

The nondimensional displacement equation can be shown to be

$$\left(\frac{dz_0}{dz_1}\right)^2 = 1 - \frac{p_h}{1/2u_0^2} + \frac{R^*}{1/2u_0^2}\left[\frac{(z_1 - z_0)^2}{2} - \int_h^{z_1} (z_1' - z_0'(z_1'))dz_1'\right], \quad (2)$$

where $R^* = \frac{1}{2}g(\gamma - B)H^2/[\frac{1}{2}g(\Delta\theta/\theta_0)H]$, and p_h is the pressure perturbation at the interface separating the density current and the upper-level rearward flow. This equation is applicable only in the far field. Since u_0 is known, the outflow speed can be obtained by using the mass continuity equation.

It can be seen that R^* has a simple physical interpretation—the convective available potential energy (CAPE) $= \frac{1}{2}g(\gamma - B)H^2$ released when a parcel is displaced from $z = 0$ to $z = H$, divided by the mean potential energy of the cold pool $\frac{1}{2}g(\Delta\theta/\theta_0)H$. Since parcels originating at $z = 0$ exit at $z = h$, it would be physically appealing to scale R^* by the quantity $\frac{1}{2}g(\Delta\theta/\theta_0)h$, which is a more precise measure of the potential energy of the cold pool, but this is inconvenient because the value of h is not fixed. We therefore retain the (external) measure of potential energy that contains the scale height H; the alternative value of R^* can be calculated a posteriori from the solutions. Also note that $R^* = F^2/F_c^2$, the ratio of the squares of the conventional Froude number for the cold pool ($F^2 = u_0^2/g(\Delta\theta/\theta)H$) to the so-called convective Froude number for the updraft ($F_c^2 = u_0^2/g(\gamma - B)H^2$). The convective Froude number is an inverse convective Richardson number, namely the ratio of the inflow kinetic energy to CAPE. Values of $R^* < 0$ represent forced ascent, and the particular case of $\gamma = 0$ represents dry adiabatic motion. Here, $R^* = 0$ represents neutrally buoyant ascent, for example, the situation in which latent heating is just sufficient to cancel the cooling effect of ascent (i.e., $\gamma = B$). Finally, $R^* > 0$ represents the situation in which the latent heating is strong enough to overcome the stratification (i.e., $\gamma > B$).

With rigid upper and lower boundary conditions, an integral constraint on the solutions is obtained by integrating the horizontal momentum equation over the domain. In nondimensional form, this gives the difference in the quantity $(u^2 + p)$ across the system

$$\int_0^1 [u^2 + p]_{-\infty}^{+\infty} dz = 0, \quad (3)$$

where "$-\infty$" and "$+\infty$" refer to asymptotic downstream and upstream values, respectively. The quantity in (3) was called the "flow–force balance" by Benjamin (1968).

The incompressible model can be interpreted in terms of height-varying density (compressibility) by transforming the vertical coordinate from height to a pressure or mass coordinate (Liu and Moncrieff 1996). In fact, in this mass coordinate the approximation that the latent heating rate is proportional to the vertical velocity should be more accurate. This transformation assures that no loss of generality is incurred by using the incompressible approximation.

3. Calm environment

First consider unsheared ambient flow in order to isolate the stratification and latent heating influences. Without loss of generality, a quiescent environment in the ground-relative sense is used to represent the far-field flow ahead of the density current, giving the system-relative environmental flow

$$u_0(z_0) = -c_0 \quad 0 \leq z_0 \leq 1, \quad (4)$$

where c_0 is the propagation speed of the density current. Note that a right-handed coordinate system is adopted

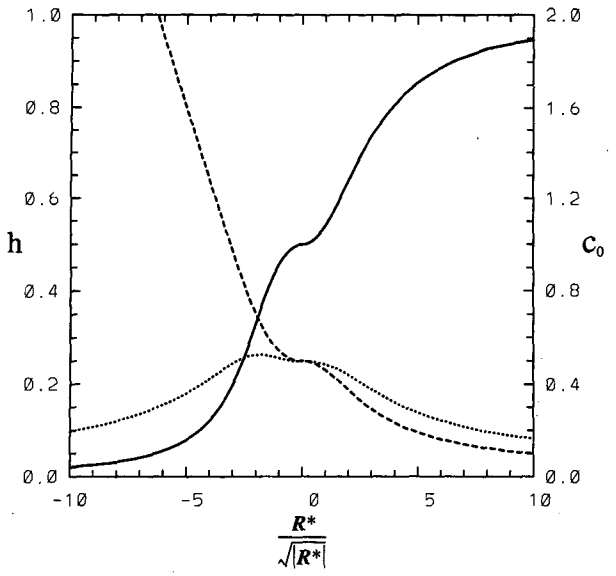

FIG. 3. Depth h (solid) and propagation speed c_0 (dashed) of the density current vs R^*. The dotted line represents the propagation speed predicted by Benjamin's formula.

with u being positive in the direction of system movement. In this situation, an analytical expression of the outflow height $z_1(z_0)$ of a streamline entering at z_0 is obtained by solving (2) while outflow (u_1) follows from mass conservation.

In the outflow region ($h \leq z_1 \leq 1$) the solutions are as follows. In the case of $R^* \leq 0$,

$$z_1 = z_0 + \frac{\epsilon_1}{\sqrt{-R^*}} \sin(\xi) - h\cos(\xi) \tag{5a}$$

and

$$u_1(z_1) = -c_0 + \epsilon_1 \cos(\xi) - \sqrt{-R^*}h \sin(\xi). \tag{5b}$$

In the case of $R^* \geq 0$,

$$z_1 = z_0 + \frac{\epsilon_2}{\sqrt{R^*}} \sinh(\zeta) - h\cosh(\zeta) \tag{5c}$$

and

$$u_1(z_1) = -c_0 + \epsilon_2 \cosh(\zeta) + \sqrt{R^*}h \sinh(\zeta), \tag{5d}$$

where $\epsilon_1 = -\sqrt{-R^*}h\cos(\alpha)/\sin(\alpha)$, $\epsilon_2 = -\sqrt{R^*}h \times \cosh(\beta)/\sinh(\beta)$, $\xi = \sqrt{-R^*}(z_1 - h)/c_0$, $\zeta = \sqrt{R^*}(z_1 - h)/c_0$, $\alpha = \sqrt{-R^*}(1 - h)/c_0$, and $\beta = \sqrt{R^*}(1 - h)/c_0$.

The pressure field is in nonhydrostatic balance except in the horizontal remote flow, where hydrostatic balance occurs. The inflow pressure perturbation is assumed to be zero, while on outflow it is

$$p(z_1) = p_h + \int_h^{z_1} g\delta\phi_1' dz_1', \tag{6a}$$

and the outflow log potential temperature perturbation is $\delta\phi_1 = (\gamma - B)(z_1 - z_0)$. Using these expressions it can be shown that if $R^* \leq 0$

$$p(z_1) = p_h - \epsilon_1 c_0[1 - \cos(\xi)] - \sqrt{-R^*}c_0 h \sin(\xi) \quad h \leq z_1 \leq 1, \tag{6b}$$

and if $R^* \geq 0$

$$p(z_1) = p_h - \epsilon_2 c_0[1 - \cosh(\zeta)] + \sqrt{R^*}c_0 h \sinh(\zeta) \quad h \leq z_1 \leq 1. \tag{6c}$$

Using (3), (4), (5), and (6), it can be shown that h and c_0 are related by

$$\frac{1}{2}h^2 + hp_h + \frac{\epsilon_1^2 c_0}{4\sqrt{-R^*}} \sin(2\alpha) - \frac{1}{4}\sqrt{-R^*}c_0 h^2 \sin(2\alpha) - \epsilon_1 c_0 h \sin^2(\alpha) = 0, \tag{7a}$$

when $R^* \leq 0$, and

$$\frac{1}{2}h^2 + hp_h + \frac{\epsilon_2^2 c_0}{4\sqrt{R^*}} \sinh(2\beta) + \frac{1}{4}\sqrt{R^*}c_0 h^2 \sinh(2\beta) + \epsilon_2 c_0 h \sinh^2(\beta) = 0, \tag{7b}$$

when $R^* \geq 0$.

By applying energy conservation along the interfacial streamline we obtain

$$p_h = \frac{1}{2}[c_0^2 + R^* h^2 - (\epsilon_1 - c_0)^2] \tag{8a}$$

for $R^* \leq 0$ and

$$p_h = \frac{1}{2}[c_0^2 + R^* h^2 - (\epsilon_2 - c_0)^2] \tag{8b}$$

for $R^* \geq 0$.

An additional relationship can be established from the hydrostatic condition within the density current and the application of the energy equation along the surface streamline, together with the assumption of a stagnation point at the leading edge

$$c_0 = [2(h + p_h)]^{1/2}, \tag{9}$$

where the quantity $(h + p_h)$ is the surface pressure in the cold pool. Expressions (7)–(9) determine how h and c_0 are formally related to R^*.

The above nonlinear equations were solved by the Newtonian iterative method, and the results are displayed as a function of R^* in Fig. 3. It can be shown

that there is a unique solution for $R^* \geq 0$, which corresponds to latent heat release. However, when $R^* < 0$, multiple solutions exist, but only the solution branch that continuously extends into the parameter range $R^* \geq 0$ is accepted. Other solutions are characterized by relatively shallower depths and slower travel speeds. The number of solutions increases as R^* decreases. Benjamin's solution ($h = 1/2$) is recovered on setting $R^* = 0$. This corresponds to either the unstratified, adiabatic situation where $B = \gamma = 0$, or neutral ascent in a stratified atmosphere in the special case when $\gamma = B$. The depth of the density current increases and the propagation speed decreases as R^* varies from negative to positive, so ascending parcels are buoyant and release potential energy. In other words, weaker stability or the addition of latent heating results in a deeper but more slowly moving density current. Conversely, a stable stratification decreases the density current depth and enhances its propagation speed.

The relationship in Fig. 3 is different from the original conservative solution of Benjamin (1968) for neutral stratification, in which the propagation speed of the density current is directly proportional to its height. This difference is ascribable to the pressure perturbation. According to (9), the propagation speed relies not only on the density current depth but also on the pressure along the interface. This is distinct from Benjamin's model and also from unstratified laboratory fluid experiments in which the upper boundary is usually a free surface and along which the pressure deviation is zero. The dependence of p_h on R^* is plotted in Fig. 4, showing that p_h decreases as the stability decreases or as latent heating increases. As a result, c_0 decreases as R^* increases, even though the density current is deeper.

The pressure perturbation at the interface is exactly nonhydrostatic when $R^* = 0$. Otherwise, the pressure can be decomposed into two parts: the dynamic (nonhydrostatic) component, which is always negative and tends to zero as $R^* \to \infty$, and the hydrostatic component. When $R^* < 0$, the nonhydrostatic component is positive and is mostly cancelled by the hydrostatic part. When $R^* > 0$ both the dynamic and thermodynamic processes generate a negative pressure deviation at the interface. As a consequence, the system translates more slowly, because the influence of the reduced pressure outweighs that due to the enhanced height. By comparison, the nonhydrostatic contribution gradually diminishes, whereas the hydrostatic pressure plays an increasingly important role when latent heating is sufficiently large to satisfy $\gamma > B$. The rearward vertical profile of pressure is marked by a low-level positive perturbation and an upper-level negative perturbation with extrema at the boundaries as $R^* < 0$ (Fig. 5a). Besides, both positive and negative pressure deviations increase with stability. As shown in Fig. 5b,

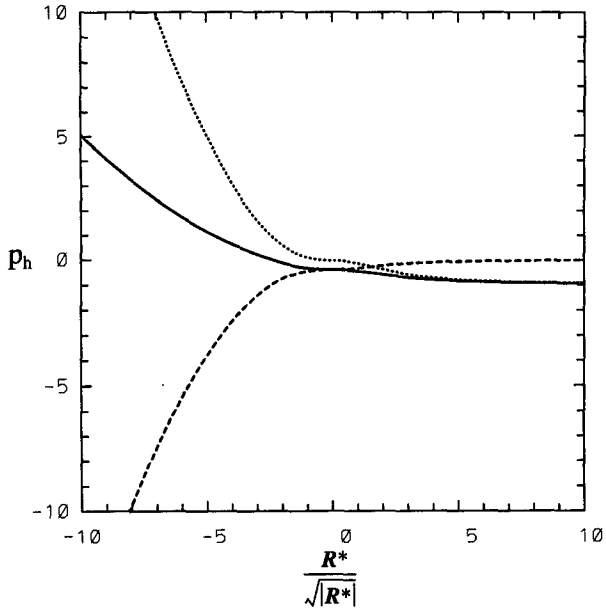

FIG. 4. The pressure perturbation at the interface (solid) versus R^*. The dotted and dashed curves represent the hydrostatic and nonhydrostatic portions, respectively.

the negative perturbation dominates through most of the depth of the model domain when $R^* > 0$, except near the lower boundary, with a minimum value at the interface.

Stratification and horizontal buoyancy gradients produced by latent heating affect the outflow shear because vorticity is baroclinically generated. It can be shown that $\eta = R^*/c_0(z_1 - z_0)$ where the y vorticity $\eta = \partial u/\partial z - \partial w/\partial x = \partial u_1/\partial z_1$. Therefore, a negative vorticity (shear) is developed at the outflow if the environment is stable. In this case, the downstream speed increases with altitude as demonstrated in Fig. 6a. The mean (negative) shear within the outflow is enhanced if R^* decreases. In contrast, the downstream flow gains positive vorticity as $R^* > 0$. The outflow speed decreases with altitude (Fig. 6b), showing a substantial enhancement near the interface and a slight reduction at the top. Using Bernoulli's principle for a neutrally stable fluid, with c_h representing the outflow velocity at the interface, it can be shown that $c_h = -\sqrt{2h}$. The downstream structure is characterized by a constant outflow that increases for deeper density currents because the outflow has to squeeze through a shallower layer. For a general stratified fluid, the interfacial outflow speed is

$$c_h = -(2h + R^*h^2)^{1/2}. \qquad (10)$$

It follows that c_h is not determined by the density-current height alone, but is reduced in a stable environment compared to a neutral one for a fixed value of h. The opposite occurs in the buoyant case (CAPE > 0).

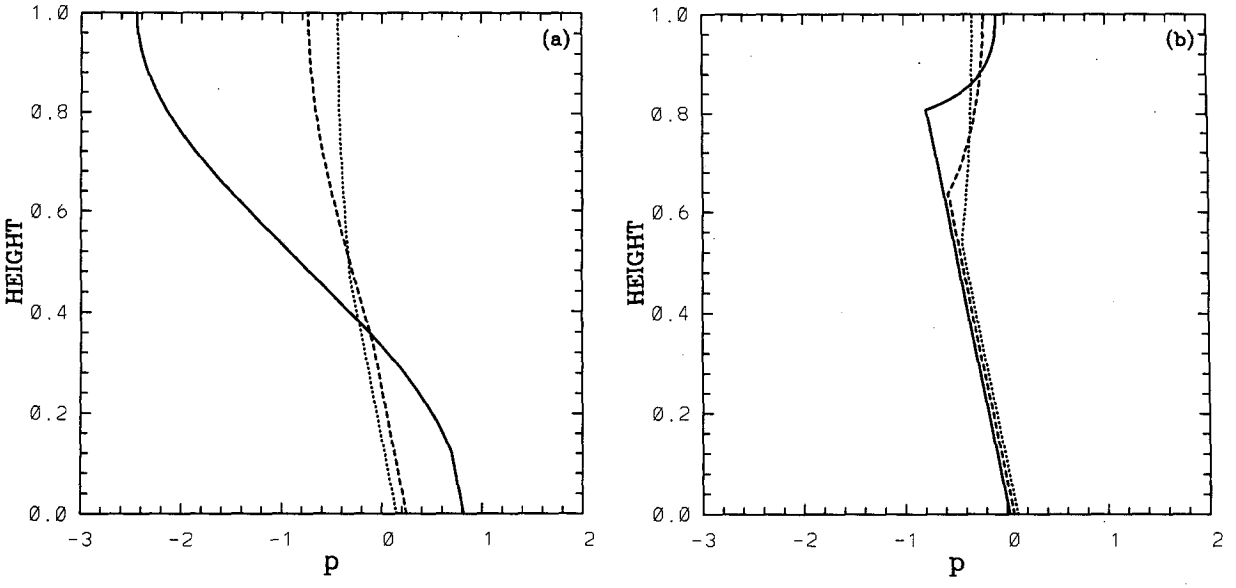

FIG. 5. The downstream pressure distribution. The solid, dashed, and dotted lines correspond to $R^* = -16$, -4, and -1, respectively, in (a) and $R^* = 16$, 4, and 1, respectively, in (b).

4. Sheared environment

For the sake of simplicity, the ambient flow is assumed to have constant shear and to be motionless at the surface. The corresponding system-relative flow, shown in Fig. 1, is described by

$$u_0(z) = c_0(Sz_0 - 1) \quad (0 \leq z_0 \leq 1), \qquad (11)$$

where S is the nondimensional shear. Due to the scaling we represent the actual shear as c_0S. Upon introducing shear, the displacement equation (2) becomes nonlinear and analytic solutions have not been obtained. The well-known numerical "shooting method" was used to obtain approximate solutions. Two boundary conditions have to be prescribed; one is clearly

$$z_0(z_1 = h) = 0. \qquad (12a)$$

The other boundary condition is straightforward provided that the shear satisfies $S \leq 1$ for an updraft current flowing rearward at every level. However, if $S > 1$ we must specify the upper boundary condition with caution. In our model an upper-level overturning circulation occurs ahead of the front when $1 < S < 2$ as shown Fig. 1. The second boundary condition is then

$$z_0(z_1 = 1) = \begin{cases} 1 & \text{for} \quad S \leq 1 \\ \dfrac{2}{S} - 1 & \text{for} \quad 1 < S < 2. \end{cases} \qquad (12b)$$

It can be shown that neutral stability in the overturning circulation is implied when the inflow speed is continuous and the base-state shear is constant.

The displacement equation (2), together with the two boundary conditions, defines a classical two-point boundary value problem. It is worth mentioning that the environmental flow defined in (11) helps satisfy the upper boundary condition (12b).

By virtue of the momentum balance condition, the following relation is established

$$(2h - 1)p_h + \frac{1}{2}h^2 + \int_h^1 [c_0^2(1 - Sz_0)^2 + R^*(z_1 - z_0)^2]dz_1 - R^* \int_h^1 \int_h^z (z_1 - z_0)dz_1 dz - c_0^2\left(1 - S + \frac{1}{3}S^2\right) = 0. \qquad (13)$$

Together with (9), this equation determines the behavior of the density current model for any ambient shear.

Figure 7 demonstrates how the height and propagation speed of density currents change with the shear parameter S for various values of R^*. Note that the model degenerates into the unstratified two-fluid model of Xu (1992) as $R^* \to 0$. Due to the different prescription of the ambient flow, however, we would not expect identical results (see Fig. 2 in Xu's paper). Regardless of the stability, some common features are noteworthy: namely, the density current deepens, and its translation is enhanced as the shear changes from negative to positive. An exception is when the stratification is very

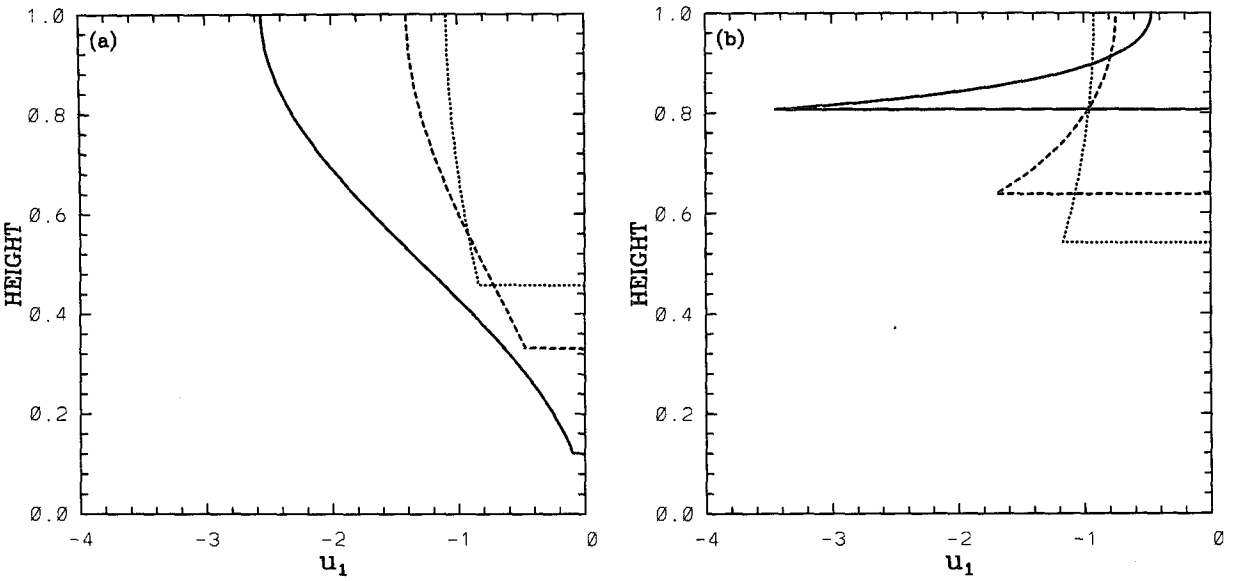

FIG. 6. The downstream wind speed distribution. The solid, dashed, and dotted lines correspond to $R^* = -16$, -4, and -1, respectively, in (a) and $R^* = 16$, 4, and 1, respectively, in (b).

stable, in which case h decreases with the shear when S exceeds a threshold value.

5. Physical aspects

Numerous atmospheric observations have shown that a thunderstorm outflow behaves like a laboratory density current in a qualitative sense. The classic equation for the propagation speed $C = \kappa\sqrt{g(\Delta\theta/\theta_0)h}$ has been widely applied to the real atmosphere, but a value of the densimetric Froude number much less than the theoretical value of $\kappa = \sqrt{2}$, derived by Benjamin (1968), is commonly used. For example, $\kappa \approx 0.75$ is used for most observed atmospheric phenomena (Wakimoto 1982) and $\kappa \approx 1$ for modeled squall lines (Nicholls et al. 1988). The issue of the appropriate value of κ has also been considered by Klemp et al. (1994). Several factors can be responsible for the inconsistency between the applied and theoretical Froude numbers, such as surface drag and internal mixing, since the theory is based upon the inviscid and frictionless idealization. We can reasonably expect that the surface friction reduces the travel speed of density currents, although this has not been precisely quantified.

Benjamin (1968) estimated the effect of energy loss due to turbulence at the interface between the cold air and the overlying fluid. The decrease in density current depth due to interfacial mixing was represented in hydraulic terms as a "head loss" parameter. He obtained the following nondimensional equation based solely on the momentum budget condition (3)

$$c_0 = \kappa\left(\frac{h(1-h)\left(1-\frac{h}{2}\right)}{(1+h)}\right)^{1/2}, \qquad (14)$$

where $\kappa = \sqrt{2}$. The maximum value of $c_0 \approx 0.53$ occurs at $h \approx 0.35$. Rottmann and Simpson (1983) examined density currents in a two-layer, time-dependent numerical channel model and found that $\kappa \approx 1$ gave the best agreement with the numerical model data.

Exactly the same expression as (14) is obtained by setting $R^* = 0$ in our conservative model, which by definition does not involve head loss. In this special case, latent heating is just sufficient to counteract the adiabatic cooling due to ascent. When we substitute our conservative solutions into (14), the propagation speed is underestimated when the fluid is statically stable but overestimated if latent heating occurs (see the dotted curve in Fig. 3). This proves that the classic density current propagation formula applied to "realistic" cases should not use constant values of the Froude number. Specifically, a Froude number smaller than $\sqrt{2}$ should be used when latent heating (condensation) occurs in the ascending air over the density current. On the other hand, a Froude number greater than the theoretical value is appropriate for density currents propagating in a stable (e.g., nocturnal) planetary boundary layer.

Highly organized narrow cold-frontal rainbands, such as those observed by James and Browning (1979), Carbone (1982), and Hobbs and Perrson

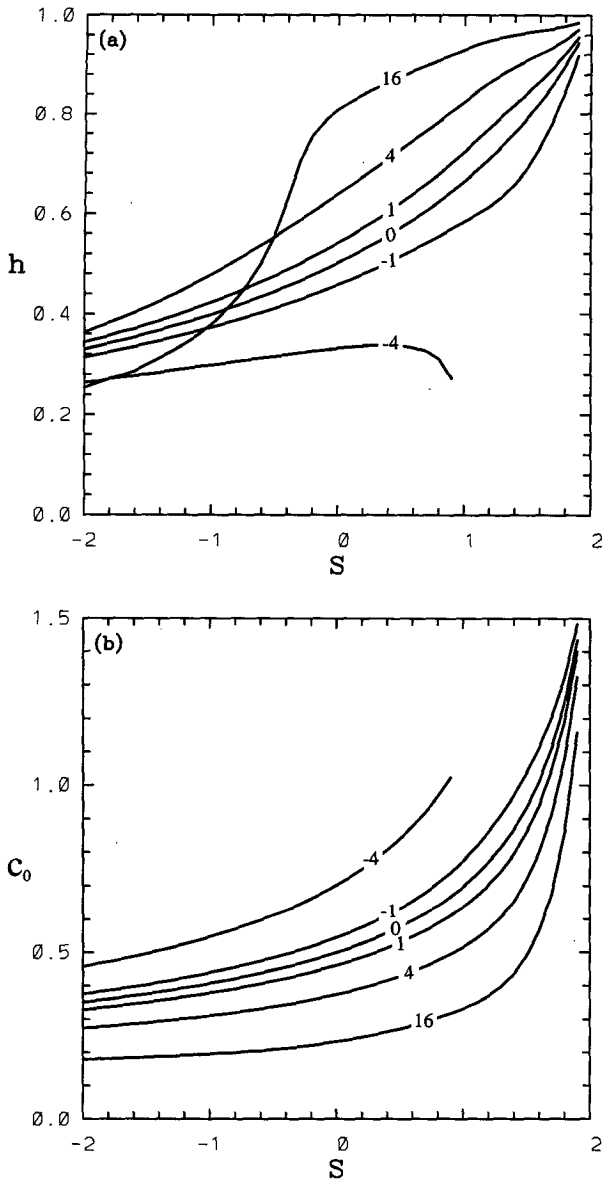

FIG. 7. Plots for different values of R^* under selected conditions. (a) Depth h of the density current vs environmental shear parameter S; (b) propagation speed c_0 versus S.

(1982), are associated with heavy precipitation, so latent heating should be taken into account in their dynamics. Since the method we use to approximate latent heating couples the thermodynamic and dynamic fields in an exact way, our analytic model represents narrow cold frontal rainbands in a more realistic way than classic density current models. For the same reason, the model could be applied to convection associated with traveling boundary-layer convergence lines, for example, those observed by radar (Wilson and Schrieber 1986).

Since we neglected rotation, our results beg the question of the role of frontogenesis. However, since the Lagrangian timescale of flow through the narrow dynamical systems we consider here is much less than the inertial timescale (i.e., a large Rossby number approximation), frontogenetic effects are expected to be minimal but are likely to be more important in wide rainbands (Testud et al. 1980).

6. Conclusions

Using a steady-state model, we showed how ambient stratification and environmental shear regulate the depth and propagation of density currents. We also examined the effects of latent heating represented in a simple way by $D\phi/Dt = w\gamma$. Noting that the atmospheric boundary layer is commonly stably stratified, an air parcel has to be displaced through a finite distance in the vertical, to its lifting condensation level, before latent heating occurs. Therefore, strictly speaking, our model applies to density currents in a saturated boundary layer since heating occurs after infinitesimal vertical displacement of fluid parcels. The analytic model could be generalized to include negatively buoyant ascent in low levels, but we expect that the conclusions would not be greatly affected.

The results reveal that a stable stratification decreases the depth of the density current and increases its propagation speed of a density current, while latent heating has the opposite effect. This result differs sharply from the classic energy conserving solution (Benjamin 1968) in which the propagation speed is proportional to its depth. This difference is due to the pressure perturbations caused by stratification and latent heating.

In constant ambient shear, it is found that the depth and propagation speed of density currents increase in positive shear, except if the stability is strong. This occurs for both adiabatic ascent in a stratified fluid and the more general situation in which latent heating occurs. Low-level shear is clearly relevant since it interacts directly with the density current interface, a problem studied by Rotunno et al. (1988). Mid- and upper-level shear can, however, have an indirect effect through the momentum budget equation. For example, a dependence on deep shear was demonstrated by Kanehisa (1993) for density currents in jetlike ambient flows.

For the most part, our analytic results are supported by the few numerical studies that have been conducted. For instance, Bischoff-Gauss and Gross (1989) showed that a density current moves faster and the head is less elevated in a stably stratified atmosphere than in the neutral situation. Haase and Smith (1989) showed that an increase in ambient static stability causes an increase in the propagation speed. The findings regarding the effect of shear are also supported by numerical modeling we have undertaken in another context (Liu

and Moncrieff 1996), although a complex transient behavior occurs in a strongly sheared ambient flow.

For simplicity, we assumed that the relative flow in the cold air was motionless, although this can be included as in Moncrieff and So (1989) and Xu and Moncrieff (1994). They showed that the cold pool dynamics enhances the propagation speed. We did not examine energy loss by nonconservative effects such as shear-induced mixing at the cold air interface. This has been shown to be relevant in studies of density currents in unstratified fluids (Benjamin 1968; Xu 1992), although classic linear perturbation theory suggests that ambient stratification and latent heating should suppress short wavelength interfacial instabilities. Finally, gravity waves can interact with the density current and significantly modify their behavior—for example, through the formation of undular bores in a strongly stratified atmosphere (Crook and Miller 1985).

An extension of this type of work is to calculate the two-dimensional flow. Note that the asymptotic solutions provide exact lateral boundary conditions for a nonlinear, two-dimensional model [see the free-boundary solution methods for fluid problems of this type devised by Moncrieff (1978) and Xu et al. (1992)]. The internal flow, pressure, and convergence fields that essentially control convection initiation can thereby be derived explicitly. Furthermore, it would be worthwhile to examine the corresponding initial-value problem in order to assess which steady states are achievable.

The significance of the upper-level overturning branch of the relative flow ahead of the system, a generalization of the stagnant region identified in Moncrieff (1989), remains to be evaluated against atmospheric observations. Its occurrence is certainly related to the vertical shear profile, in particular, to ambient flow conditions having moderate ambient shear in upper levels and strong shear in low levels. Note that a different type of organization—a blocking or choking of the front-to-rear airflow branch—is linked to weak upper-level shear (Liu and Moncrieff 1996).

Finally, we point to the need for new observations with which to evaluate the role of latent heating and shear on density currents and similar phenomena, noting that little attention has been paid to these aspects in previous field experiments.

Acknowledgments. The authors express their appreciation to Dr. Andrew Crook and Prof. Roger Smith for their comments, and to M. Currie for carefully editing the manuscript.

REFERENCES

Benjamin, T. B., 1968: Gravity currents and related phenomena. *J. Fluid Mech.*, **31,** 209–248.

Bischoff-Gauss, I., and G. Gross, 1989: Numerical studies on cold fronts. Part I: Gravity flows in a neutral and stratified atmosphere. *Meteor. Atmos. Phys.*, **40,** 150–158.

Britter, R. E., and J. E. Simpson, 1978: Experiments on the dynamics of a gravity current head. *J. Fluid Mech.*, **88,** 223–240.

Carbone, R. E., 1982: A severe frontal rainband. Part I: Stormwide hydrodynamic structure. *J. Atmos. Sci.*, **39,** 258–279.

Charba, J., 1974: Application of gravity current model to analysis of squall-line gust front. *Mon. Wea. Rev.*, **102,** 140–156.

Clarke, R. H., 1961: Mesostructure of dry cold fronts over featureless terrain. *J. Meteor.*, **18,** 715–735.

Crook, N. A., and M. J. Miller, 1985: A numerical and analytical study of atmospheric undular bores. *Quart. J. Roy. Meteor. Soc.*, **111,** 225–242.

Goff, R. C., 1976: Vertical structure of thunderstorm outflows. *Mon. Wea. Rev.*, **104,** 1429–1440.

Haase, S. P., and R. K. Smith, 1989: The numerical simulation of atmospheric gravity currents. Part II: Environments with stable layers. *Geophys. Astrophys. Fluid Dyn.*, **46,** 35–51.

Hobbs, P. V., and P. O. B. Persson, 1982: The mesoscale and microscale structure and organization of clouds and precipitation in midlatitude cyclones. Part V: The substructure of narrow cold-frontal rainbands. *J. Atmos. Sci.*, **39,** 280–295.

James, P. K., and K. A. Browning, 1979: Mesoscale structure of line convection at surface cold fronts. *Quart. J. Roy. Meteor. Soc.*, **105,** 371–382.

Kanehisa, H., 1993: Density currents in jet shear flows. *J. Meteor. Soc. Japan,* **71,** 633–636.

Klemp, J. B., R. Rotunno, and W. C. Skamarock, 1994: On the dynamics of gravity currents in a channel. *J. Fluid Mech.*, **269,** 169–198.

Liu, C.-H., and M. W. Moncrieff, 1996: A numerical study of the effects of ambient flow and shear on density currents. *Mon. Wea. Rev.*, **124,** 2282–2303.

Moncrieff, M. W., 1978: The dynamical structure of two-dimensional steady convection in constant vertical shear. *Quart. J. Roy. Meteor. Soc.*, **104,** 543–567.

——, 1981: A theory of organized steady convection and its transport properties. *Quart. J. Roy. Meteor. Soc.*, **107,** 29–50.

——, 1989: Analytical models of narrow cold-frontal rainbands and related phenomena. *J. Atmos. Sci.*, **46,** 150–162.

——, and J. S. A. Green, 1972: The propagation and transfer properties of steady convective overturning in shear. *Quart. J. Roy. Meteor. Soc.*, **98,** 336–352.

——, and D. W. K. So, 1989: A hydrodynamical theory of conservative bounded density currents. *J. Fluid Mech.*, **198,** 177–197.

Nicholls, M. E., R. H. Johnson, and W. R. Cotton, 1988: The sensitivity of two-dimensional simulations of tropical squall lines to environmental profiles. *J. Atmos. Sci.*, **45,** 3625–3649.

Nielsen, J. W., and P. P. Neilley, 1990: The vertical structure of New England coastal fronts. *Mon. Wea. Rev.*, **118,** 1793–1807.

Rottmann, J. W., and J. E. Simpson, 1983: Gravity currents produced by instantaneous releases of a heavy fluid in a rectangular channel. *J. Fluid Mech.*, **135,** 95–110.

Rotunno, R., J. B. Klemp, and M. L. Weisman, 1988: A theory for long-lived squall lines. *J. Atmos. Sci.*, **45,** 463–485.

Shapiro, M. A., T. Hampel, D. Rotzoll, and F. Mosher, 1985: The frontal hydraulic head: A micro-α scale (1 km) triggering mechanism for mesoconvective weather systems. *Mon. Wea. Rev.*, **113,** 1166–1183.

Simpson, J. E., 1969: A comparison between laboratory and atmospheric density currents. *Quart. J. Roy. Meteor. Soc.*, **95,** 758–765.

——, and R. E. Britter, 1979: The dynamics of the head of a gravity current advancing over a horizontal surface. *J. Fluid Mech.*, **94,** 477–495.

——, and ——, 1980: A laboratory model of an atmospheric mesofront. *Quart. J. Roy. Meteor. Soc.*, **106,** 485–500.

Smith, R. K., and M. J. Reeder, 1988: On the movement and low-level structure of cold fronts. *Mon. Wea. Rev.*, **116,** 1927–1944.

Testud, J., G. Berger, P. Amayenc, M. Chong, B. Nutten, and A. Sauvaget, 1980: A Doppler radar observation of a cold front: Three-dimensional air circulation, related precipitation system and associated wavelike motions. *J. Atmos. Sci.*, **37,** 78–98.

Wakimoto, R. M., 1982: The life cycle of thunderstorm gust fronts as viewed with Doppler radar and rawinsonde data. *Mon. Wea. Rev.*, **110,** 1060–1082.

Wilson, J. W., and W. E. Schrieber, 1986: Initiation of convective storms by radar-observed boundary layer convergence lines. *Mon. Wea. Rev.*, **114,** 2516–2536.

Xu, Q., 1992: Density currents in shear flows—A two-fluid model. *J. Atmos. Sci.*, **49,** 511–524.

——, and M. W. Moncrieff, 1994: Density current circulations in shear flows. *J. Atmos. Sci.*, **51,** 434–446.

——, F. S. Chang, and C. P. Lou, 1992: Finite element solutions of free-interface density currents. *Mon. Wea. Rev.*, **120,** 230–233.